High-Speed Pulse Transmission along a Slow-Wave CPW for Monolithic Microwave Integrated Circuits

CHING-KUANG C. TZUANG, MEMBER, IEEE, AND TATSUO ITOH, FELLOW, IEEE

Abstract—**High-speed pulse transmission along a coplanar waveguide (CPW) integrated on a monolithic microwave integrated circuit (MMIC) is analyzed. The time-domain waveform is obtained by the inverse discrete Fourier transform (IDFT) of the frequency-domain data, namely, complex characteristic impedance and propagation constant. The full-wave mode-matching method (MMM) is employed to analyze the dispersion of the CPW. A simple wide-band matching scheme is found to be effective to make the slow-wave CPW a viable circuit element in applications such as a delay line or an interconnection line.**

I. INTRODUCTION

ADVANCES IN monolithic microwave integrated circuits (MMIC's) and picosecond devices have continuously improved the switching speed of the active devices and pushed real-time high-speed signal processing into the picosecond range [1], [2]. For operating speeds higher than gigabits per second, the conventional lumped capacitance approximation of an interconnection line in an MMIC may no longer be accurate. Instead, field-theoretical considerations are required in the logic, circuit, and layout of very high speed integrated circuits [3]. In addition to the propagation delay, it is important to know the actual signal waveform after its propagation along an interconnection line which connects both the source and the load. This is because the waveform parameters such as rise time, fall time, settling time, overshoot, and preshoot play a fundamental role in the success of a very high speed digital or wide-band analog integrated circuit. The signal degradations stemming from the dispersive characteristics and improper terminations of a slow-wave coplanar waveguide (CPW) integrated on an MMIC will be discussed in this paper.

The CPW has also become an important transmission line element in MMIC technologies because of its easy access for the ground plane, reduction in crosstalk between adjacent transmission lines, and lower radiation at discontinuities as compared to a microstrip line [4], [5]. When a CPW becomes part of an integrated circuit, slow-wave propagation may occur. Planar metal–insulator-semiconductor (MIS) and Schottky contact CPW's were examined and the existence of slow-wave propagation was both experimentally and theoretically confirmed [6], [7]. As the physical dimensions of the CPW become smaller, the finite conductor thickness of a CPW is no longer negligible. Therefore, it is clear that only accurate field calculations of a CPW can result in accurate simulation of an ultra-high-speed narrow pulse transmission on an MIS or Schottky contact slow-wave CPW.

It was reported that severe signal degraduations can occur for pulse transmission along a well-matched semi-infinite lossless microstrip line and a CPW for distances less than 1 cm [8]–[10]. The case of pulse transmission with the possible existence of slow-wave propagation was reported in [11]–[13]. The purpose of this paper is to present a detailed analysis of pulse transmissions on an MIS or Schottky contact CPW integrated in a microcircuit under various kinds of input excitations and arbitrary combinations of source and load terminations. First, frequency-domain characteristics of the slow-wave CPW are obtained. A hybrid TE and TM full-wave analysis based on the mode-matching method (MMM) is applied to our model, shown in Fig. 1. Once the complex propagation constant is obtained, the field distributions inside a slow-wave CPW are known. The Poynting power and currents flowing on the surface of the signal (or center) conductor of a CPW can be obtained by integrations. This leads to the determination of the complex characteristic impedance based on the power–current definition. The validity of the accuracy of the characteristic impedance defined by the power–current definition is checked against that obtained by the power–voltage definition based on the spectral-domain analysis (SDA).

After the accuracy is confirmed, the inverse discrete Fourier transform (IDFT) is invoked to convert the frequency-domain data for a CPW connected with a source and a load into time-domain waveforms. It is found that an impedance matching scheme can be useful in making slow-wave CPW a good interconnection line or a delay line with very little degradation on the propagating waveform.

Manuscript received July 17, 1986; revised April 11, 1987. This work was supported in part by the Office of Naval Research under Contract N00014-79-C-0553.

C.-K. C. Tzuang was with the Department of Electrical and Computer Engineering, University of Texas at Austin. He is now with the Institute of Communication Engineering, National Chiao Tung University, Hsin Chu, Taiwan.

T. Itoh is with the Department of Electrical and Computer Engineering, University of Texas at Austin, Austin, TX 78712.

IEEE Log Number 8715413.

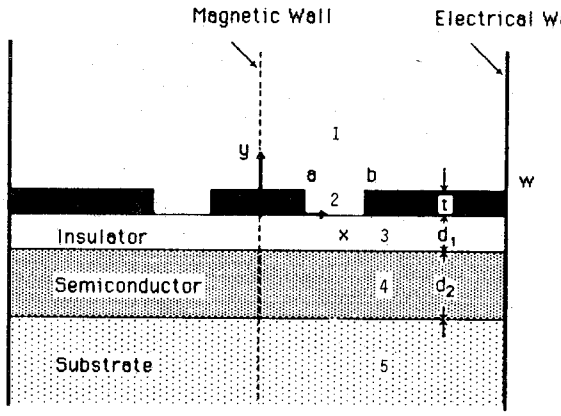

Fig. 1. The slow-wave coplanar waveguide model.

II. Model and Method of Analysis

A. Physical Model

The slow-wave CPW model shown in Fig. 1 was used for the analysis. The coplanar waveguide with finite conductor thickness is located on top of a layered structure. It consists of metal, insulator (or depletion region for Schottky contact), semiconducting layer (or epitaxial layer), and semi-insulating substrate. By setting the conductivity of the semiconductor layer to zero, Fig. 1 may represent a conventional lossless CPW. This model is general enough to analyze most CPW's integrated in MMIC. By knowing the integrated circuit (IC) processing data and physical dimensions, one should be able to compute the time-domain pulse waveform propagating on such a CPW.

B. Frequency-Domain Analysis

The mode-matching method which has been widely used to analyze various waveguide structures [14], [15] was applied to the frequency-domain analysis of the slow-wave CPW shown in Fig. 1. The technique itself does not result in a unique formulation for the same problem. Instead, many possible formulations can yield the same solution for the propagation constant. Because of the even symmetry for the propagating mode of interest, a magnetic wall is placed at the center of the guide. Electric walls are placed at a large distance to simplify the analysis [7]. The modal field expansions in each region shown in Fig. 1 can be expressed in terms of TE-to-y and TM-to-y Hertzian potentials. For instance, the potential functions in region 1 are

$$\psi^1(x,y)=\sum_{m=1}^{M} A_m\cos(\beta_m x)\,e^{-\alpha_{1m}(y-t)}$$

$$\phi^1(x,y)=\sum_{m=1}^{M} B_m\sin(\beta_m x)\,e^{-\alpha_{1m}(y-t)}$$

$$\beta_m=(2m-1)\pi T/2w;\ \alpha_{1m}^2-\gamma^2-\beta_m^2+\omega^2\mu_0\epsilon_0\epsilon_{R1}=0. \quad (1)$$

In region 2, the potential functions are

$$\psi^2(x,y)=\sum_{n=2}^{N}\sin[\beta_{2n}(x-a)]\{C_n\sin(\alpha_{2n}y)+\tilde{C}_n\cos(\alpha_{2n}y)\}$$

$$\phi^2(x,y)=\sum_{n=1}^{N}\cos[\beta_{2n}(x-a)]\{D_n\sin(\alpha_{2n}y)+\tilde{D}_n\cos(\alpha_{2n}y)\}$$

$$\beta_{2n}=(n-1)\pi/(b-a);\ \alpha_{2n}^2+\beta_{2n}^2+\gamma^2=\omega^2\mu_0\epsilon_0\epsilon_{R2} \quad (2)$$

where $\epsilon_{Ri}=\epsilon_i-j\sigma_i/\omega\epsilon_0$, and ϵ_i and σ_i are the relative dielectric constant and conductivity of the ith dielectric layer, respectively, with $\sigma_i=0$ except for $i=4$. The potential functions in regions 3 through 5 can be derived in a similar way such that they satisfy the boundary conditions imposed by the radiation condition and by both magnetic wall and electric walls.

By matching the adjacent tangential fields in regions 3 through 5 and applying the orthogonality relationships between potential functions, the coefficients of the modal field expansions in these regions can be eliminated. Next, we match the adjacent tangential fields in regions 1 through 3 at $y=0$ and $y=t$, respectively. Finally, a homogeneous matrix equation of dimension $(2N-1)$ by $(2N-1)$ can be derived:

$$\begin{bmatrix} P_{mn}(\gamma) & \vdots & Q_{mn}(\gamma) \\ \cdots & \cdots & \cdots \\ R_{mn}(\gamma) & \vdots & S_{mn}(\gamma) \end{bmatrix}\begin{bmatrix} C_2 \\ \dot{C}_n \\ \ddot{D}_1 \\ \dot{\tilde{D}}_n \end{bmatrix}=0 \qquad (AX=0). \quad (3)$$

The expressions for $P_{mn}(\gamma)$, $Q_{mn}(\gamma)$, $R_{mn}(\gamma)$, and $S_{mn}(\gamma)$ are functions of the unknown complex propagation constant γ. To obtain a nontrivial solution for the column vector X of (3), part of the unknown coefficients of the modal field expansions in region 2, the determinant of matrix A has to be zero. The real and imaginary parts of γ correspond to the slow-wave factor (λ_0/λ) and the attenuation constant, respectively, λ_0 being the free-space wavelength.

C. Complex Characteristic Impedance

Once the complex propagation constant γ is obtained, the unknown field coefficients C_n and D_n are found within a constant multiplicative factor. The field distributions in each region are solved immediately. Based on the power–current definition, the characteristic impedance is

expressed as

$$Z_0 = \frac{\int_S \vec{E}_t \times \vec{H}_t \cdot \vec{n}\, da}{|I_t|^2} = \frac{1}{2} \frac{\sum_{k=1}^{5} \int_{Sk} (E_{kx} H_{ky}^* - E_{ky} H_{kx}^*)\, da_k}{\left| \int_0^a (H_{3x})_{y=0}\, dx + \int_0^t (H_{2y})_{x=a}\, dy - \int_0^a (H_{1x})_{y=t}\, dx \right|^2} \tag{4}$$

where the subscript k denotes the subregion k, and S is the cross-sectional area of the CPW.

D. Time-Domain Analysis

An equivalent linear 2-port ABCD matrix representation of the CPW can be applied to derive the complex transfer function, at a distance z from the source, of the terminated slow-wave CPW shown in Fig. 2 at each incremental angular frequency step. The transfer function can be written in terms of γ and z_0 as

$$\frac{V_0(n\omega)}{V_s(n\omega)} = \frac{Z_{1\text{eff}}(n\omega)}{\{\cos(\gamma z) Z_{1\text{eff}}(n\omega) + jZ_0 \sin(\gamma z) + [j \sin(\gamma z) Z_{1\text{eff}}(n\omega)/Z_0 + \cos(\gamma z)] Z_s\}}$$

$$Z_{1\text{eff}}(n\omega) = \frac{\cos[\gamma(L-z)] Z_L + jZ_0 \sin[\gamma(L-z)]}{j \sin[\gamma(L-z)] Z_L/Z_0 + \cos[\gamma(L-z)]} \tag{5}$$

where n is an integer.

The corresponding time-domain function is recovered by means of a standard inverse discrete Fourier transform (IDFT) procedure. Both a rectangular pulse of finite rise and fall times and a Gaussian pulse of finite width are applied to analyze time-domain waveforms. Note that the case for a lossless, well-matched, and semi-infinitely long transmission line is a special case obtained by setting $Z_L = Z_0$ and $Z_s = 0$ in (5).

III. Frequency-Domain Solutions

Figs. 3(a) and 3(b) are plots of the normalized propagation constant and the characteristic impedance of an MMIC CPW with both undoped and lightly doped epitaxial layers. To check the accuracy of the present mode-matching method (MMM), the results for a lossless (undoped) CPW with extremely thin metallization (with the conductor thickness one hundredth of the half center strip width a) have been compared with those by the spectral-domain method (SDA). The latter can handle only the structure with an infinitely thin conductor ($t = 0$). The normalized propagation constants (slow-wave factors) obtained by the two methods differ by less than 0.5 percent. The results of the characteristic impedance by the MMM cannot be distinguished on the graph from those by the SDA, identified as curve (1) on Fig. 3(b).

As the conductor thickness is increased, both the slow-wave factor and the characteristic impedance decreased. Fig. 3 also shows the case with a thin semiconducting epitaxial layer which has finite resistivity of 10 $\Omega \cdot$cm corresponding to an n-type GaAs substrate with a light doping level of 10^{14} cm^{-3} [16].

The dispersion characteristics in Fig. 3(a) indicate that the CPW's with the structure parameters chosen here retain the quasi-TEM nature up to a frequency of around 100 GHz. The discrepancy of the characteristic impedance data shown in Fig. 3(b) above 100 GHz is not caused by a physical mechanism, but rather by the definitions used. In the case of SDA, the power–voltage definition is used. The voltage is calculated as the integration of the electric field across the slot. On the other hand, the power–current definition is used for the MMM in this paper. This choice is due to the fact that in the SDA the formulation starts with the slot field while in the MMM the current on the center strip can easily be found from the discontinuity of the magnetic field. Data by the two definitions are basically indistinguishable up to 100 GHz. This fact further indicates that a quasi-TEM approximation can be used up to 100 GHz for these specific structures which are consistent with the findings in Fig. 3(a).

Another slow-wave CPW structure with smaller dimensions is analyzed. The results are shown in Fig. 4 for both slow-wave factor and attenuation constant versus frequency. The physical dimensions are chosen to comply with the current integrated circuit technology. The real and imaginary parts of the characteristic impedance are shown in Fig. 5.

IV. Time-Domain Results

When a slow-wave CPW is excited by a rectangular pulse of 80-ps (picosecond) rise and fall times (measured by 10–90 percent rise or fall) and 300 ps wide with zero source impedance and a 10-fF (femtofarad) load, a damped oscillatory output waveform is observed (Fig. 6). Fig. 6 is obtained by means of IDFT (inverse discrete Fourier transform) that converts the frequency-domain data of Figs. 4 and 5 from 0.1 GHz to 20 GHz at 0.1-GHz incremental frequency steps. When the output load capacitance (C_L) is increased from 10 fF to 80 fF, the output waveform is almost identical. This fact suggests that the output loading has little effect on the oscillation and that the slow-wave CPW itself has inductive, capacitive, and resistive components. As the transient voltage waveform is excited at the input end of the CPW, the spike will occur

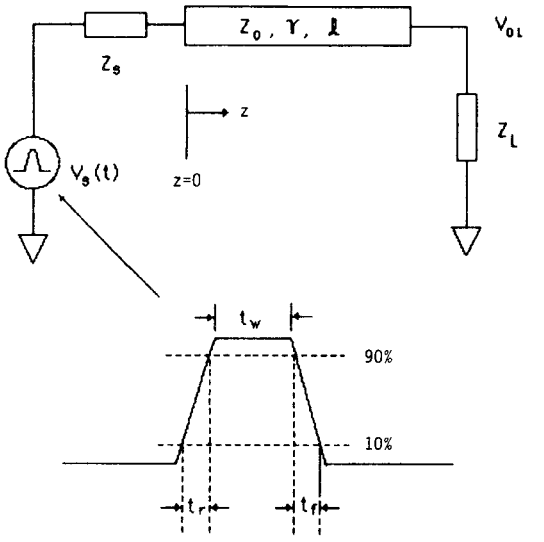

Fig. 2. Equivalent circuit representation of a slow-wave CPW.

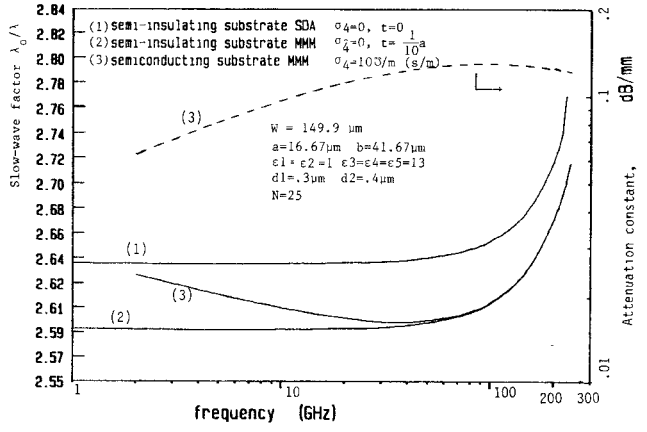

(a)

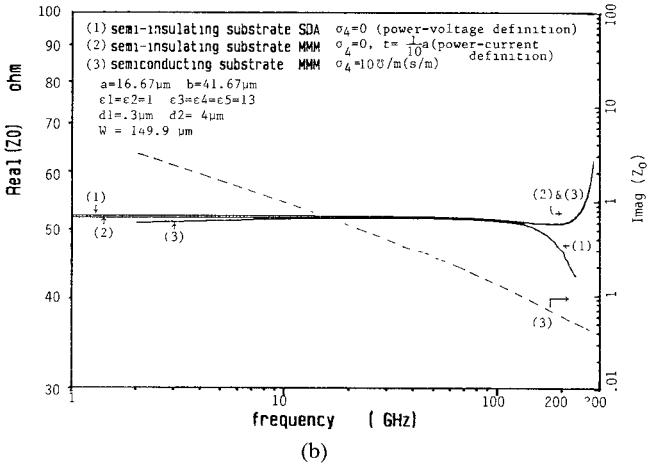

(b)

Fig. 3. Propagation constant and characteristic impedance versus frequency obtained by both MMM and SDA methods. The results by MMM for $t = a/100$ cannot be distinguished on the graphs from the SDA results (1). (a) Slow-wave factor (solid line) and attenuation constant (dashed line) versus frequency. (b) Real and imaginary parts of the characteristic impedance versus frequency for the same CPW with dimensions shown in Fig. 3(a).

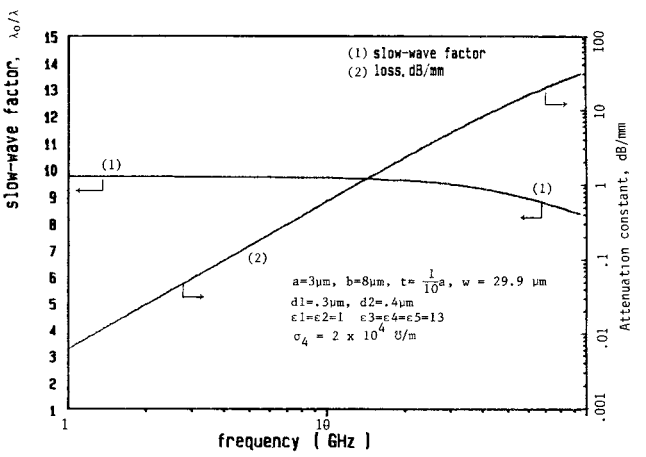

Fig. 4. Slow-wave factor and attenuation constant versus frequency for an MMIC CPW with a heavily doped epitaxial layer.

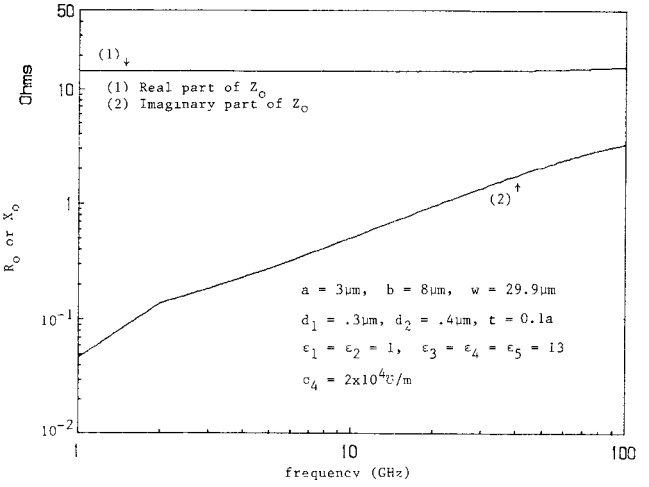

Fig. 5. Real and imaginary parts of the characteristic impedence versus frequency for the same CPW shown in Fig. 4.

just as in the case of an inductor. Once the input excitation is settled to a dc voltage, the slow-wave CPW has to reach the final steady state in a damped oscillation manner because the slow-wave propagation of this type usually exhibits a large capacitance in the low-frequency limit [17] and the CPW itself is lossy, as shown in Fig. 4.

Referring to Fig. 8, the case to be discussed later, one will find that the propagation delay per unit length for the same slow-wave CPW structure is approximately 350 ps/cm. The corresponding propagation delay of the slow-wave CPW analyzed in Fig. 6 is 350 ps/cm $\times$ 1 cm/10 mm $\times$ 1.5 mm = 53 ps. On the other hand, the rise and fall times of the input pulse excitation are 80 ps, which is larger than 53 ps. As a result, the output waveform, curve (2) at the load end in Fig. 6, shows little delay. This is actually close to 50 ps, as illustrated in Fig. 6, noting that one half of the smaller division is 50 ps, and is excited almost instantaneously by the input pulse if one considers it has considerably slow rising and falling edges, 80-ps rise and fall times, and a wide pulse width (300 ps).

It is then plausible to consider that the results obtained in Fig. 6 can be explained by lumped circuit approxima-

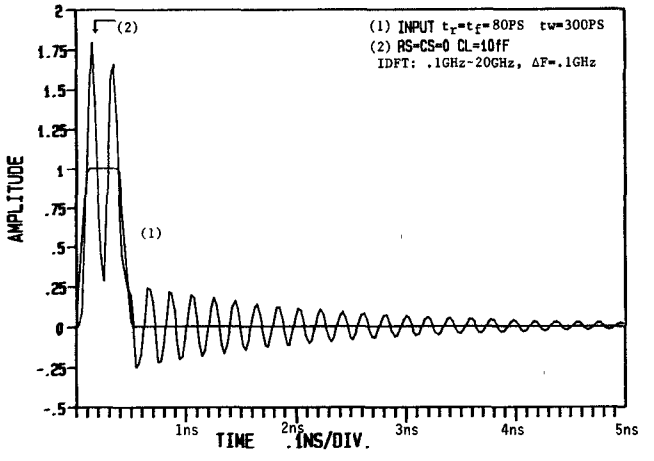

Fig. 6. Transient excitation of a slow-wave CPW with frequency-domain data shown in Figs. 4 and 5 with a short-circuited input and a capacitive load ($l = 1.5$ mm).

tions. A simple calculation based on the equivalent *RLC* circuit of the slow-wave CPW, Fig. 7(a), can estimate the damping factor k and predict the second peak approximately.

In terms of normalized coordinates, the maximum and minimum responses of the circuit model (Fig. 7(a)) to a unit step input occur at [18]

$$x_m = m/2(1-k^2)^{1/2} \quad y_m = 1-(-1)^m \exp(-2\pi k x_m) \tag{6}$$

where

$$x_m = \omega_0 t/2\pi \quad y_m = v_0(t) \quad \omega_0 = \frac{1}{\sqrt{LC_2}} \text{ and } k = \frac{\omega_0 L}{2R_2}.$$

It follows that

$$y1 = 1.8 = 1-(-1)\exp\left[-k/(1-k^2)^{1/2}\right]$$

for $m = 1$, the first peak, that the damping factor $k \cong 0.071$, and that

$$y_3 = 1-(-1)^3 \exp\left[\left(-3k/(1-k^2)^{1/2}\right] = 1.5\right.$$

for $m = 3$, the second peak. The second peak in Fig. 6 is 1.65, which is 10 percent away from the quick estimations based on the simple *RLC* model.

From the theory of a uniform transmission line, the characteristic impedance $Z_0 = R_0 + jX_0 = (Z/Y)^{1/2}$, and the propagation constant $\gamma = \alpha + j\beta = (ZY)^{1/2}$. Thus, we should obtain four nonlinear equations for the component values of the slow-wave CPW model. To avoid iterative numerical solutions for these unknowns, a linearized set of equations are listed:

$$R_0 \cong (L/C_2)^{1/2} \tag{7}$$

$$X_0 \cong 0.5 R_0 g_2/\omega C_2 \tag{8}$$

$$\lambda_0/\lambda = \text{slow-wave factor} = 3\times 10^8 (LC_2)^{1/2} \tag{9}$$

$$g_2/C_2 = 6\times 10^8 A_c/\left[(\lambda_0/\lambda)8.6859\times 10^{-3}\right] \tag{10}$$

where A_c = the attenuation constant (dB/mm) = $8.6859\times 10^{-3}\cdot\alpha$. However, these linearized equations (7)–(10) are not all independent. Combining (7) and (9), one may calculate L (inductance per unit length) and C_2 (effective capacitance per unit length). The ratio of g_2 to C_2 can be determined from (10), and the value of X_0 can be computed by (8) to check against that shown in curve (2) of Fig. 5.

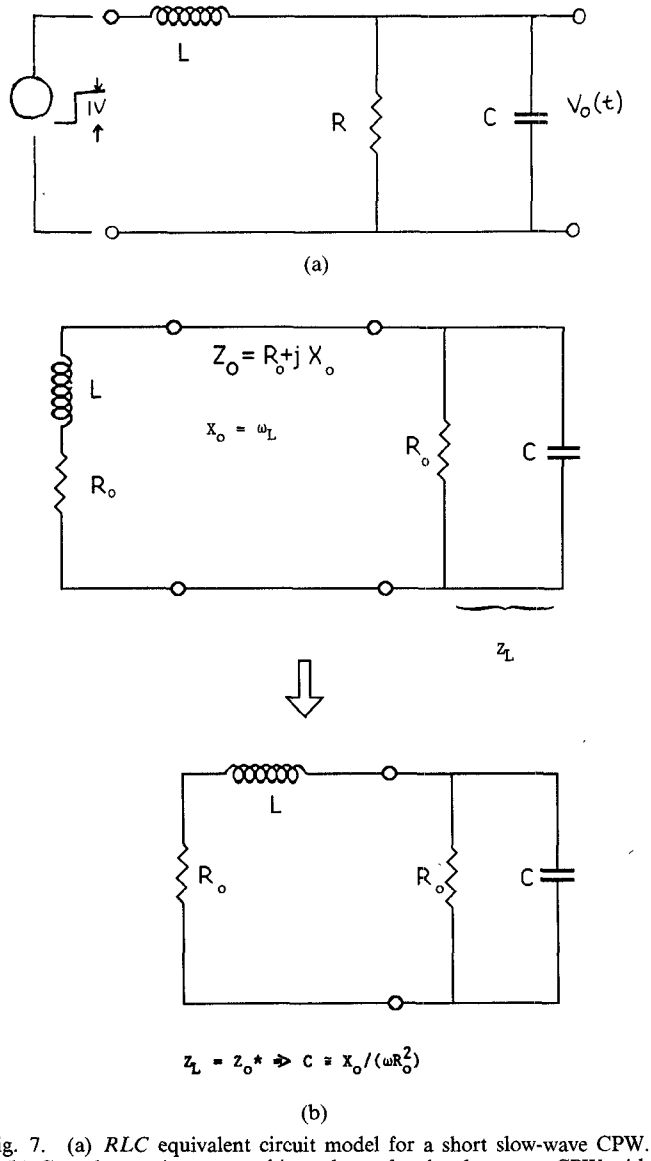

Fig. 7. (a) *RLC* equivalent circuit model for a short slow-wave CPW. (b) Complex conjugate matching scheme for the slow-wave CPW with complex characteristic impedance shown in Fig. 5.

Some numerical results are $L = 4.83\times 10^{-7}$ H/m and $C_2 = 2.299\times 10^{-9}$ F/m. At 1 GHz,

$$g_2 = 0.127 \ll [\omega c_2 = 14.445].$$

At 10 GHz,

$$g_2 = 9.53 \ll [\omega c_2 = 144.45].$$

At 20 GHz,

$$g_2 = 38.6 \ll [\omega c_2 = 288.9].$$

Note that the estimated values of X_0, the imaginary part of Z_0, at 1 GHz, 10 GHz, and 20 GHz by means of the simplified equivalent circuit model and those of the com-

TABLE I
COMPARISONS OF X_0, THE IMAGINARY PART OF Z_0, OBTAINED BY THE THEORETICAL MODE-MATCHING METHOD AND THE EQUIVALENT *RLC* MODEL

Frequency (GHz)	X_0 (Ω) [equivalent circuit model]	X_0 (Ω) [Fig. 5]	k [damping factor]
1	0.063	0.0466	0.00138
10	0.478	0.509	0.104
20	0.955	0.954	0.414

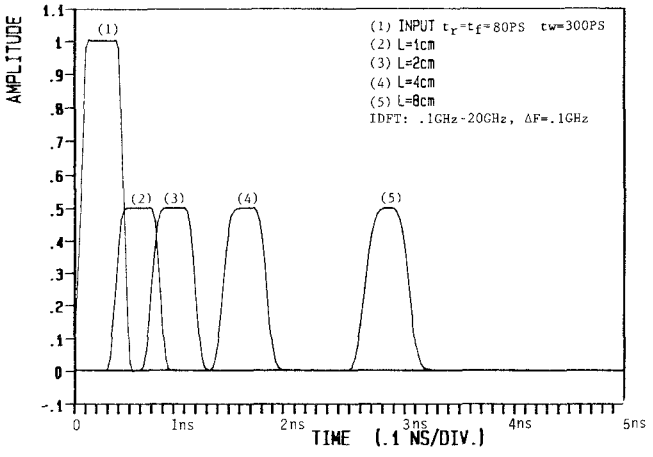

Fig. 8. Transient pulse waveforms with matched source and load terminations for the slow-wave CPW's with lengths ranging from 1 cm to 8 cm.

puted X_0 based on the mode-matching method (Fig. 5) are tabulated for comparison (Table I). It is clear that solutions from both the equivalent circuit model and the MMM are consistent.

To make the slow-wave CPW a useful MMIC element requires good wide-band matching circuits. Ideally, if both source and load impedances are complex conjugately matched to the complex characteristic impedance ($Z_0 = R_0 + jX_0$) of the CPW at each incremental frequency, the oscillations associated with the transient input excitation will be suppressed according to the theory of complex normalization of scattering parameters [19]. If the imaginary part of the characteristic impedance of the MMIC CPW is positive (reactive), then that of the source or load matching circuit should be negative (susceptive) to have a matched termination. Therefore, it is evident that a simple parallel resistor and capacitor (RC) network can be applied as a wide-band matching circuit for the CPW under study provided the value of the capacitor does not change too much in the frequency band of interest. This idea is illustrated in Fig. 7(b):

$$Z_{L(R//C)} = R_0/(1 + j\omega CR_0)$$
$$\cong R_0 - j\omega CR_0^2 = R_0 - jX_0$$

provided $\omega CR_0 \ll 1$.

Under the assumption that the value of X_0 is much smaller than that of R_0, one can obtain the expression for the value of C, the capacitor of the parallel RC matching

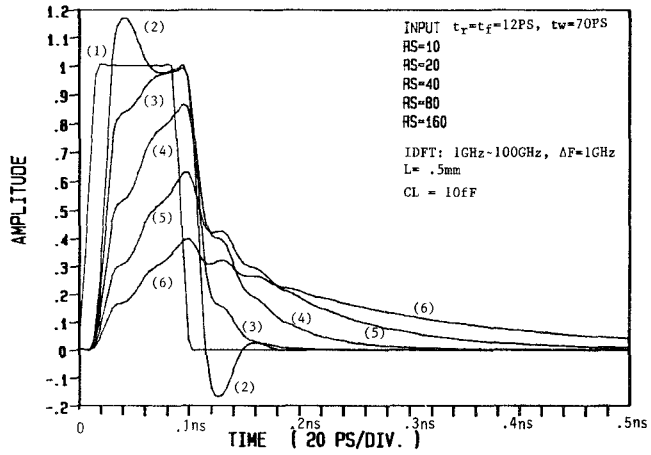

(a)

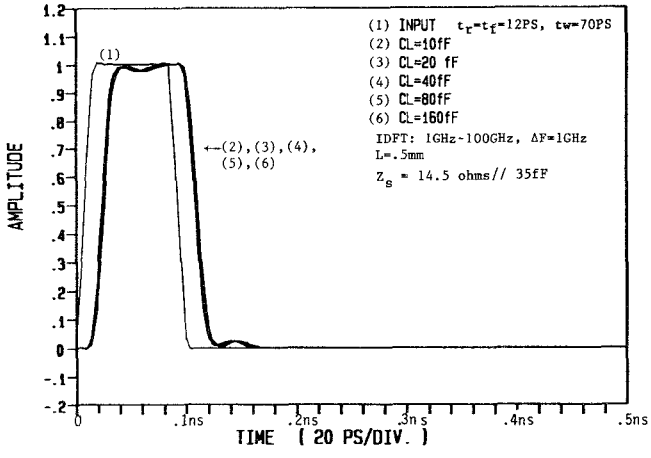

(b)

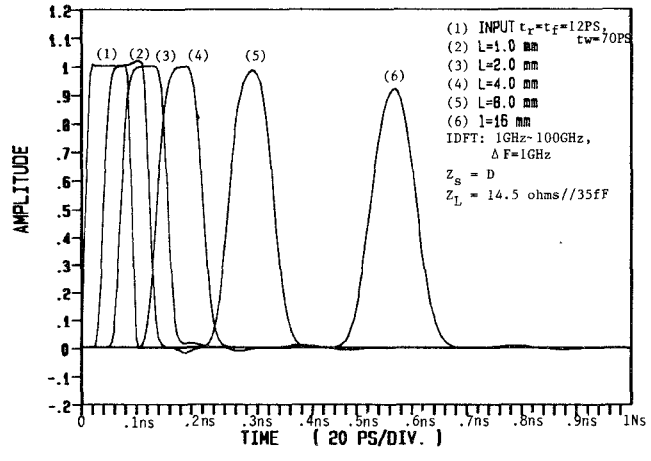

(c)

Fig 9. Transient pulse excitations on the slow-wave CPW with frequency-domain data shown in Figs. 4 and 5. (a) Transient pulse excitations with resistive source and capacitive load terminations. (b) Transient pulse excitations with matched source and capacitive load terminations. (c) Transient pulse excitations with short-circuited source and matched load terminations.

circuit:

$$C \cong X_0/(\omega R_0^2) \tag{11}$$

where ω is the angular frequency.

Examining curve (2) of Fig. 5, it is evident that the imaginary part (X_0) of the characteristic impedance Z_0 is

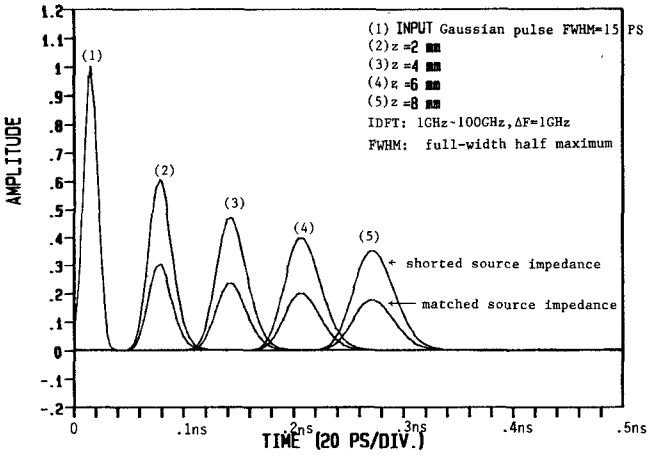

Fig. 10. Transient Gaussian pulse excitations with a matched output load and matched or short-circuited source terminations for a 10-mm-long CPW with frequency-domain data shown in Figs. 4 and 5.

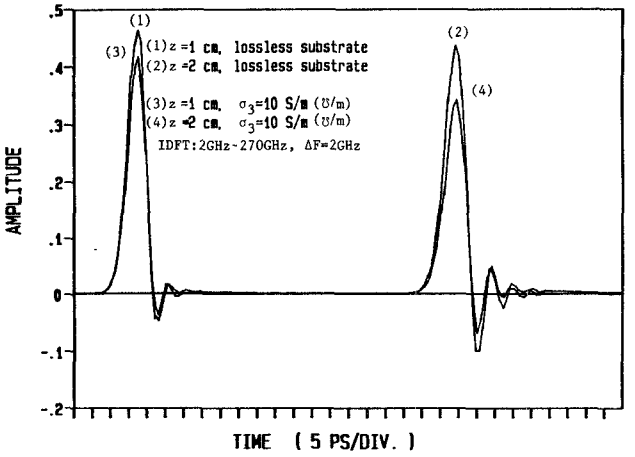

Fig. 11. Gaussian pulse transmission along lossless or low-loss CPW's under matched terminations with and without semiconducting layer at different locations of the CPW's.

approximately proportional to the angular frequency. This suggests that a constant value of C can be employed for wide-band matching since C is proportional to the ratio of X to ω (eq. (11)). Detailed calculations show that the value of C starts from 35 fF, stays relatively constant till 20 GHz, and then declines gradually to 25 fF at 100 GHz. In what follows, a parallel RC circuit comprising a 14.5 Ω resistor and a 35-fF capacitor is employed for matching the specific MMIC CPW with complex characteristic impedance.

Under the matched source and load terminations, Fig. 8 shows that the rectangular pulse can propagate 8 cm with little degradation and is delayed by approximately 2.6 ns. The ringing shown in Fig. 6 is completely suppressed.

Next, the MMIC CPW is excited with a rectangular pulse with smaller rise and fall times, 12 ps. Under the unmatched terminations, the output waveform can have overshoot or preshoot with some ringing (ripple) superimposed on it as shown in Fig. 9(a) depending on the value of the source resistance [13]. When the input source is matched, the output waveform has very little degradation for driving an output capacitive load up to 160 fF as shown in Fig. 9(b). Fig. 9(c) displays the dispersion of a rectangular pulse for different lengths of the CPW with zero (short-circuited) source impedance and a matched output load.

Finally, the case of a low-loss semiconducting layer is examined. Fig. 10 shows the propagation of a Gaussian pulse of 15 ps FWHM (full-width at half maximum) with a matched output load and either a short-circuited or a matched input source termination. The results shown in curve (3) of Fig. 3(a) and (b) actually correspond to such a case. These data imply that there exists no slow-wave mode or mode transition in the structure under analysis since the imaginary part of the complex characteristic impedance is very small and approaches zero at higher frequencies. Fig. 11, obtained by converting the frequency-domain data shown in curve (2) of Fig. 3(a) and (b) into the time-domain waveform, compares the results of a Gaussian pulse of 5-ps FWHM observed 1 cm and 2 cm from the source end for substrate with and without semiconducting layer. In this CPW structure, the effect of the semiconducting layer with small conductivity or low doping concentration attenuates the pulse waveform and alters the shape of the Gaussian pulse in a way similar to those reported in [8]–[10] for the cases of a microstrip and a CPW.

V. Conclusions

Time-domain response of picosecond pulse transmission along a slow-wave MIS or Schottky contact CPW is presented. Severe drawbacks such as overshoot, preshoot, and ringing in applying the slow-wave CPW [12], [13] are eliminated almost entirely by an appropriate wide-band impedance matching technique proposed in this paper. As a result, a slow-wave CPW can be a useful interconnection line or a delay line in MMIC's provided careful matching between the slow-wave transmission line and terminations is practiced. All of these applications are analyzed separately with examples in the time domain. We may anticipate that other slow-wave structures, such as an MIS microstrip line and MIS coupled microstrip lines, should exhibit similar properties found in this paper. The theoretical approach presented in this paper proves to be a versatile tool for the solutions of very high speed pulse transmission on an MMIC CPW.

References

[1] C. P. Lee, P. L. Miller, D. Hou, and R J. Anderson, "Ultra high speed integrated circuits using GaAs/GaAlAs high mobility transistors," in *Proc. Device Research Conf.* paper IIA-7, June 1983.

[2] R. K. Jain, K. Stenersen, and D. E. Snyder, "Picosecond optoelectronics in high-speed integrated circuits," *Proc. SPIE*, vol. 439, pp. 174–176, 1983.

[3] H. Hasegawa and S. Seki, "Analysis of interconnection delay on very high speed LSI/VLSI chips using an MIS microstrip line model," *IEEE Trans. Microwave Theory Tech.*, vol. MTT-32, pp. 1721–1727, Dec. 1984.

[4] M. Riaziat, I. Zubeck, S. Bandy, and G. Zdasiuk, "Coplanar waveguides used in 2–18 GHz distributed amplifier," in *IEEE MTT-S Int. Microwave Symp.*, June 1986, pp. 337–338.

[5] R. W. Jackson, "Coplanar waveguide vs. microstrip for millimeter wave integrated circuits," in *IEEE MTT-S Int. Microwave Symp.*, June 1986, pp. 699–702.
[6] H. Hasegawa and H. Okizaki, "M.I.S. and Schottky slow-wave coplanar stripline on GaAs substrate," *Electron. Lett.*, vol. 13, pp. 663–664, Oct. 1977.
[7] Y. Fukuoka, Y. C. Shih, and T. Itoh, "Analysis of slow-wave coplanar waveguide for monolithic integrated circuits," *IEEE Trans. Microwave Theory Tech.*, vol. MTT-31, pp. 567–573, July 1983.
[8] K. K. Li, G. Arjavalingam, A. Dienes, and J. R. Whinnery, "Propagation of picosecond pulses on microwave striplines," *IEEE Trans. Microwave Theory Tech.*, vol. MTT-30, pp. 1270–1273, Aug. 1982.
[9] G. Hasnain, A. Dienes, and J. R. Whinnery, "Dispersion of picosecond pulses in coplanar transmission lines," *IEEE Trans. Microwave Theory Tech.*, vol. MTT-34, pp. 738–741, June 1986.
[10] R. L. Veghte and C. A. Balanis, "Dispersion of transient signals in microstrip transmission lines," in *IEEE MTT-S Int. Microwave Symp. Dig.*, pp. 691–694, June 1986.
[11] C. Seguinot, P. Kennis, P. Pribetich, and J. F. Legier, "Crosstalk phenomenon in coupled microstrip lines laid on semi-conducting substrates," in *15th European Microwave Conf. Dig.*, (Paris), Sept. 1985, pp. 826–830.
[12] C.-K. Tzuang and T. Itoh, "Pulse transmission on a slow-wave MIS and Schottky coplanar waveguide with finite conductor thickness," in *15th European Microwave Conf. Dig.*, (Paris), Sept. 1985, pp. 225–230.
[13] C.-K. Tzuang and T. Itoh, "Pulse transmission in an interconnection line on a semiconductor substrate with a lossy layer," in *1985 VLSI Multilevel Interconnection Conf. Dig.*, (Santa Clara, CA), June 25–26, pp. 424–430.
[14] R. Mittra, Y. L. Hou, and V. Jamnejad, "Analysis of open dielectric waveguides using mode-matching technique and variational methods," *IEEE Trans. Microwave Theory Tech.*, vol. MTT-28, pp. 36–43, Jan. 1980.
[15] G. Kowalski and R. Pregla, "Dispersion characteristics of shielded microstrips with finite thickness," *Arch. Elek. Übertragung*, vol. 25, no. 5, pp. 193–196, Apr. 1971.
[16] S. M. Sze, *Physics of Semiconductor Devices*, 2nd ed. New York: Wiley, 1981, p. 33.
[17] H. Ogawa and T. Itoh, "Slow-wave characteristics of ferromagnetic semiconductor microstrip lines," in *IEEE MTT-S Int. Microwave Symp. Dig.*, June 1986, pp. 65–68.
[18] J. Millman and C. Halkias, *Integrated Electronics: Analog and Digital Circuits and Systems*, New York: McGraw-Hill, 1972, pp. 453–456.
[19] N. Balabania and T. A. Bickart, *Electrical Network Theory*. New York: Wiley, 1969, p. 614.

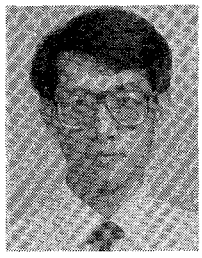

Ching-Kuang C. Tzuang (S'84–M'87) was born in Taiwan on May 10, 1955. He received the B.S. degree in electronic engineering from the National Chiao Tung University, Hsin Chu, Taiwan, in 1977 and the M.S. degree from the University of California at Los Angeles in 1980.

From February 1981 to June 1984, he was employed at TRW, Redondo Beach, CA, working on high-speed and monolithic microwave integrated circuits. He received the Ph.D. degree in electrical engineering in 1986 from the University of Texas at Austin, where he worked on high-speed transient analyses of monolithic microwave integrated circuits under the supervision of Dr. T. Itoh. Since September 1986, he has been with the Institute of Communication Engineering, National Chiao Tung University, Hsin Chu, Taiwan, R.O.C. He is currently conducting research on optical millimeter-wave and microwave techniques.

✠

Tatsuo Itoh (S'69–M'69–SM'74–F'82) received the Ph.D. degree in electrical engineering from the University of Illinois, Urbana, in 1969.

From September 1966 to April 1976, he was with the Electrical Engineering Department, University of Illinois. From April 1976 to August 1977, he was a Senior Research Engineer in the Radio Physics Laboratory, SRI International, Menlo Park, CA. From August 1977 to June 1978, he was an Associate Professor at the University of Kentucky, Lexington. In July 1978, he joined the faculty at the University of Texas at Austin, where he is now a Professor of Electrical and Computer Engineering and Director of the Electrical Engineering Research Laboratory. During the summer of 1979, he was a guest researcher at AEG-Telefunken, Ulm, West Germany. Since September 1983, he has held the Hayden Head Centennial Professorship of Engineering at the University of Texas. Since September 1984, he has been Associate Chairman of Research and Planning of the Electrical and Computer Engineering Department.

Dr. Itoh is a member of the Institute of Electronics and Communication Engineers of Japan, Sigma Xi, and Commission B of USNC/URSI. He was Editor of the IEEE TRANSACTIONS ON MICROWAVE THEORY AND TECHNIQUES for 1983–1985, and serves on the Administrative Committee of the IEEE Microwave Theory and Techniques Society. He is a Professional Engineer registered in the state of Texas.